American Journal of Modern Physics
2026, Vol. 15, No. 5, pp. 148–161
https://doi.org/10.11648/j.ajmp.20261505.12

SciencePG
Science Publishing Group

Research Article

Compact Correlated Hylleraas Wave Functions for the Lithium Isoelectronic Sequence: Ground-State Energies and a Complex-Rotation Assessment

Youssou Gning, Mame Diarra Dieng, Moussa Toure, Demba Sylla, Mamadou Lamine Samb*

Department of Physics and Chemistry, Iba Der Thiam University of Thies, Thies, Senegal

Abstract

The nonrelativistic ground-state energy of the $(1s^22s)^2S$ term of atomic lithium and five members of its isoelectronic sequence (Be^+, B^{2+}, C^{3+}, N^{4+}, O^{5+}; Z = 3–8) is computed with a correlated Hylleraas-type trial function combined with the complex-rotation (complex-scaling) transformation of the radial coordinates, implemented symbolically and numerically in the computer-algebra system Maxima. Two variational basis sizes, Ω = 9 and Ω = 12, are compared for neutral lithium as a sensitivity test of the complex-scaled stabilization procedure; Ω = 9 gives the closer benchmark agreement and is used as the working basis for the ionic members of the sequence. The resulting energies agree with the multiple-basis-set Hylleraas benchmark of Yan, Tambasco and Drake with relative deviations below 6.1×10^{-3}% over Z = 3–8, and with several independent Hylleraas, full-core-plus-correlation, and screening-constant calculations reported in the literature. The evolution of the optimized non-linear parameters with nuclear charge is examined and interpreted in terms of the progressive contraction of the $1s^2$ core relative to the comparatively stable 2s valence orbital. Because the $(1s^22s)^2S$ term lies below the first ionization threshold rather than embedded in the continuum, the small imaginary parts produced by the complex-rotation procedure cannot be interpreted as a physical autoionization width; this limitation of applying a resonance-oriented technique to a genuine bound state is discussed explicitly. The present implementation is placed in the context of an earlier complex-rotation study of the same states by Diop et al. (2020), to which it is methodologically related but numerically independent.

Keywords

Lithium Isoelectronic Sequence, Complex Rotation, Hylleraas Wave Functions, Correlated Variational Calculation, Three-Electron Atoms, Ground-State Energy, Maxima

1. Introduction

Among the many-electron atomic systems tractable for detailed variational study, the lithium atom and its isoelectronic ions occupy a distinctive position: with three electrons bound to a nucleus of charge Z, they combine a closed $1s^2$ core with a single valence electron, and the sequence introduces three interelectronic terms (r_{12}^{-1}, r_{13}^{-1}, r_{23}^{-1}) rather than the single term of the two-electron helium sequence, while remaining

*Correspondence: Mamadou Lamine Samb (mlsamb@univ-thies.sn)

Received: 3 September 2026; **Accepted:** 11 September 2026; **Published:** 27 September 2026

small enough for accurate, physically interpretable wave functions. Lithium-like ions are also benchmark systems in atomic spectroscopy and plasma modelling.

The theoretical study of these systems has a long history, from the orbital calculations of the 1930s to the sub-microhartree Hylleraas-type expansions of Yan, Drake and collaborators, the full-core-plus-correlation method of Chung and coworkers, and the compact Hylleraas bases of Thakkar and coworkers [1-8]. These studies converge on a ground-state energy of neutral lithium near −7.478060 hartree, known to better than one part in 10^{11} [9, 10], and on comparably precise energies for the ionic members of the sequence. Recent studies continue to explore compact explicitly correlated representations and high-accuracy relativistic treatments across the lithium isoelectronic sequence, confirming the continuing methodological interest in these systems [11, 12].

A separate strand concerns atomic resonances embedded in the continuum, for which bound-state variational methods do not apply. The complex-rotation transformation, established by Aguilar and Combes and by Balslev and Combes [13, 14] and reviewed extensively [15, 16], rotates the radial coordinates into the complex plane and exposes a resonance as an isolated complex eigenvalue $W = E_r - i\Gamma/2$ detached from the rotated continuum. It has been applied to two- and three-electron doubly-excited states, including by the Dakar–Thies atomic-physics school built around the work of Wague, Biaye, Gning and coworkers [16-23].

The present work applies this machinery, with a compact Hylleraas-type correlated trial function, to the $(1s^2 2s)^2S$ ground state of lithium and five isoelectronic ions (Be^+, B^{2+}, C^{3+}, N^{4+}, O^{5+}). Because this term lies below the ionization threshold, complex rotation is not strictly required to obtain its energy; it is used here as a methodological validation, since the ground-state energy is independently known to high precision and offers a transparent benchmark for the correlated basis, rotated-coordinate machinery and Maxima implementation intended for future work on genuine autoionizing resonances, including a check of where its resonance-oriented output ceases to carry physical meaning (Sec. 5.5). A directly related precedent exists: Diop, Gning and coworkers [24] applied complex rotation with a differently constructed Hylleraas basis to the same ground state and to excited $(1s^2ns)^2S$ states up to Z = 20. Independent calculations by Wang, Zhu and Chung [25] also reported energies for the excited $1s^2ns$ states (n=3,4, and 5) of the lithium isoelectronic sequence, providing additional literature data for this class of three-electron systems. The present study is methodologically related but uses a distinct compact architecture, is restricted to Z = 3–8, and was implemented independently in Maxima; Ref. [24] is treated as the closest methodological point of comparison; no quantitative claim of greater basis compactness relative to that work is made here because the two basis constructions use different counting conventions.

The paper proceeds as follows: Sec. 2 presents the Hamiltonian and correlated basis; Sec. 3 the complex-rotation formalism; Sec. 4 the Maxima implementation; Sec. 5 the energies, basis-size sensitivity, literature comparison, parameter trends, and the interpretation of the residual imaginary component; Sec. 6 concludes.

2. Three-Electron Hamiltonian and Correlated Basis

2.1. The Nonrelativistic Three-Electron Hamiltonian

In the infinite-nuclear-mass, nonrelativistic approximation, the Hamiltonian of a three-electron atomic system of nuclear charge Z (in Hartree atomic units) is

$$H = -\frac{1}{2}(\Delta_1 + \Delta_2 + \Delta_3) - Z\left(\frac{1}{r_1}+\frac{1}{r_2}+\frac{1}{r_3}\right) + \frac{1}{r_{12}}+\frac{1}{r_{13}}+\frac{1}{r_{23}} \quad (1)$$

where r_i is the distance of electron i from the nucleus and $r_{ij} = |r_i - r_j|$ the interelectronic separations. The last three terms couple the electronic coordinates and prevent an exact separation of variables for any Z once more than one electron is present; this is the essential difficulty that a correlated variational treatment must address, and it becomes more severe for the three-electron case than for helium because three independent pair-correlation terms, rather than one, enter the wave function simultaneously [26, 27].

2.2. Correlated Hylleraas-type Trial Function

Following the strategy introduced by Hylleraas for helium [1] and its subsequent extension to three-electron systems [2-6, 20, 24], the correlated basis used to represent the $(1s^2 2s)^2S$ state is built from individual basis functions, each carrying explicit exponential and polynomial dependence on r_1, r_2, r_3 and on the three interelectronic distances, multiplied by an angular–spin factor that couples the two 1s core electrons to the 2s valence electron with the required doublet spin symmetry and total orbital angular momentum L = 0. A single basis function, labelled by six non-negative integers (i, j, k, n, p, q), is written explicitly as

It is convenient to denote the six-integer label of a basis function by $\mu \equiv$ (i, j, k, n, p, q). A single basis function is then written explicitly as

$$\varphi_\mu(r_1, r_2, r_3) = r_1^{\,i}\, r_2^{\,j}\, r_3^{\,k}\, exp - (\lambda_1 r_1 + \lambda_2 r_2 + \lambda_3 r_3) \times r_{12}^{\,n}\, r_{13}^{\,p}\, r_{23}^{\,pr} \times \chi(r_1, r_2, r_3) \quad (2)$$

where i, j, k are the powers of the individual radii r_1, r_2, r_3; n, p, q are the powers of the interelectronic distances r_{12}, r_{13}, r_{23}; λ_1, λ_2 (with $\lambda_1 = \lambda_2$ imposed in the present work, Sec. 4) are the non-linear screening parameters associated with the two 1s core electrons and λ_3 the parameter associated with the 2s valence electron; and χ is the angular–spin factor discussed in Sec. 2.4, which combines the spherical harmonics of the three electrons to total orbital angular momentum L = 0 and couples their spins to the doublet (S = ½) required for the ground state. The six integers making up μ are restricted to a single fixed total, i + j + k + n + p + q = Ω, which defines the size Ω of the variational basis: every admissible non-negative integer tuple μ contributes exactly one basis function φ_μ of the form above, and the full trial wave function is the linear combination.

$$\Psi(r_1,r_2,r_3) = \Sigma_\mu c_\mu \varphi_\mu(r_1, r_2, r_3),$$

summed over all $\mu = (i, j, k, n, p, q)$

with $i + j + k + n + p + q = \Omega$,

with the linear coefficients c_μ determined variationally (Sec. 3.2) for each fixed set of non-linear parameters (λ_1, λ_2, λ_3, θ).

Physically, this construction reflects a picture in which the two innermost electrons form a helium-like core around the nucleus, and the third electron interacts with that dressed core much as a single satellite particle orbits a compound hydrogen-like system: a decomposition that is only approximate, since all three electrons remain fully coupled through the r_{12}, r_{13} and r_{23} terms of Eq. (1), but that is nonetheless useful for interpreting the physical trends reported in Sec. 5.4. Figure 1 sketches this core–satellite picture, and Figure 2 shows the full set of radial and interelectronic Hylleraas coordinates that enter the trial function of Eq. (2).

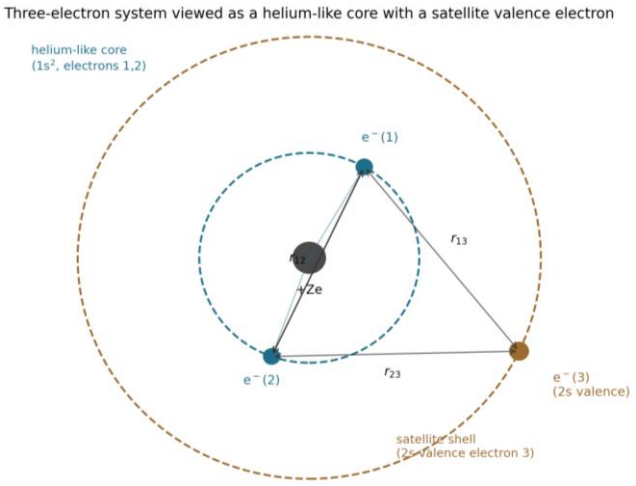

Figure 1. *The three-electron system pictured as a helium-like $1s^2$ core (electrons 1, 2) accompanied by a satellite 2s valence electron (electron 3), together with the three interelectronic distances that couple the two shells.*

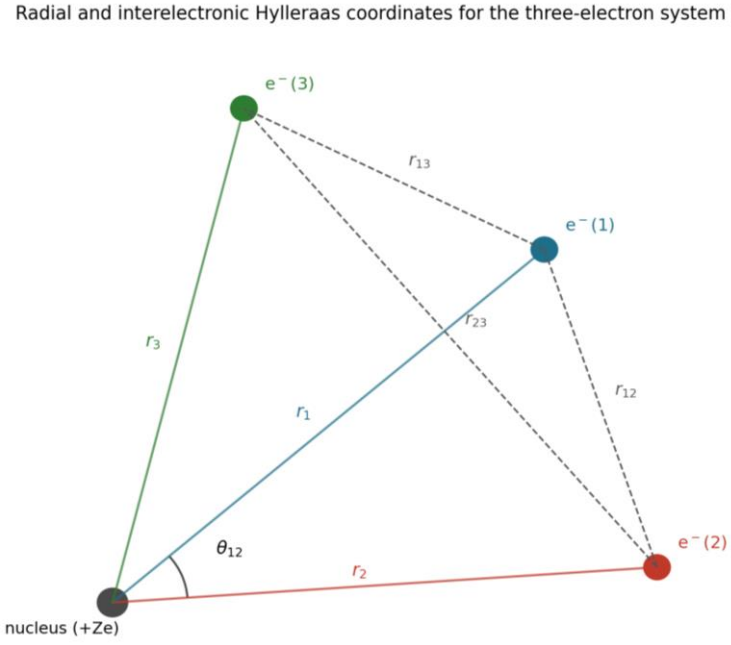

Figure 2. *Radial coordinates r_1, r_2, r_3 and interelectronic distances r_{12}, r_{13}, r_{23} entering the correlated Hylleraas basis of Eq. (2); θ_{12} denotes the angle between r_1 and r_2.*

2.3. Matrix Elements

The normalization integral and the matrix elements of the kinetic-energy, nuclear-attraction and electron–electron repulsion operators between two basis functions of the form (2) reduce, after separation of the angular and spin parts, to finite sums of radial integrals over r_1, r_2, r_3 with integrands built from powers of these coordinates, of the interelectronic distances, and of the exponentials $e^{-\lambda_i r_i}$. Because the interelectronic distances r_{ij} cannot themselves be expanded in a simple closed form when the angular integration is carried out, each r_{ij}^c factor entering the trial function is re-expressed through its Legendre/Gegenbauer expansion in the two radii r_i, r_j and the enclosed angle, following the standard Hylleraas machinery; the resulting radial integrals are of confluent-hypergeometric type and were evaluated symbolically, term by term, rather than approximated numerically. This reduction to fully analytic radial integrals, as opposed to numerical quadrature, is what makes an implementation in a computer-algebra environment such as Maxima practical for the present basis sizes (Sec. 4), since it removes the discretization error that would otherwise be introduced by numerical integration over three radial coordinates.

Explicitly, for two radii $r_a \le r_b$ the power $r_{ab}^c \equiv |r_a - r_b|^c$ admits the multipole expansion

$$r_{ab}{}^c = 4\pi \sum_l \frac{1}{(2\ell+1)} a_l^c(r_a, r_b) \; Y_l(\Omega_a) \cdot Y_l(\Omega_b) \qquad (3)$$

with the radial coefficient $a_l^c(r_a,r_b)$ expressible through a Gauss hypergeometric function ${}_2F_1$ of the ratio $(r_a/r_b)^2$. For positive integer powers arising from the Hylleraas correlation factors, particular coefficients can simplify algebraically; the $c = 1$, $\ell = 0$ case is worked out explicitly below. The electron–electron Coulomb operator is handled separately through the standard Laplace expansion of $1/r_{ab}$ in powers of $r_</r_>$ multiplied by Legendre polynomials. This expansion is not assumed to terminate. For each pair of basis functions, it is combined with the polynomial factors already present in the bra and ket, and the angular-momentum selection rules leave a finite set of contributions to the matrix element. Thus, the Coulomb-repulsion term is not evaluated by assuming truncation of a $c = -2$ hypergeometric series. After the angular integrations are carried out analytically, the surviving terms reduce to finite sums of radial integrals of the generic form given in Eq. (4).

$$\int_0^\infty \int_0^\infty \int_0^\infty r_1^a r_2^b r_3^c \, exp - (\lambda_1 r_1 + \lambda_2 r_2 + \lambda_3 r_3) \, dr_1 \; dr_2 \; dr_3 \qquad (4)$$

for integer exponents a, b, c fixed by the tuple (i, j, k, n, p, q) of the two basis functions being combined and by the derivative order (0, 1 or 2) contributed by the kinetic-energy operator acting on either function. Each such integral factorizes into a product of three one-dimensional integrals of the elementary form $\int_0^\infty r^m \; e^{-\lambda r} \; dr = m!/\lambda^{(m+1)}$ for non-negative integer m, so that the full matrix element is ultimately a rational function of $\lambda_1, \lambda_2, \lambda_3$ (and, once complex rotation is switched on, of the rotated combinations $e^{-i\theta}\lambda_i$ in place of λ_i, introduced in Sec. 3.1 below). It is this fully closed-form structure, rather than any numerical approximation of the radial integrals, that is generated symbolically for every pair of basis functions and subsequently assembled into the Hamiltonian and overlap matrices of Sec. 4.

To make this reduction concrete, it is worth working it through explicitly for the simplest non-trivial pair of basis functions, since this is the type of analytic expression that Maxima generates and combines for every pair of basis functions at a given Ω. Consider the two uncorrelated, lowest-order radial factors obtained from Eq. (2) by setting all six exponents (i, j, k, n, p, q) to zero except for a single unit power on r_{12},

$$\phi_0(r_1, r_2, r_3) = exp - (\lambda_1 r_1 + \lambda_2 r_2 + \lambda_3 r_3), \; \phi_1(r_1, r_2, r_3) = r_{12} \; exp - (\lambda_1 r_1 + \lambda_2 r_2 + \lambda_3 r_3) \qquad (5)$$

Each function is multiplied by the angular–spin factor χ of Eq. (2), whose normalized angular contribution is omitted here for brevity. The overlap $\langle\phi_1|\phi_0\rangle$ requires the expansion of r_{12} in Eq. (3) with $c = 1$. For the s-symmetric overlap only the $\ell = 0$ component survives the angular integration. Writing $r_>$ $= \max(r_1,r_2)$ and $r_< = \min(r_1,r_2)$, the exact coefficient is $a_0^1(r_1,r_2) = r_> [1 + (r_</r_>)^2/3] = r_> + r_<^2/(3r_>)$, not $r_>$ alone. The additional term contributes at the same inverse-length order and therefore cannot be neglected. With this coefficient, Eq. (6) follows.

$$\langle\phi^1|\phi^0\rangle = \int_0^\infty \int_0^\infty \int_0^\infty r_1 2 r_2 2 r_3 2 \; [r_> + \frac{r_<^2}{3r_>}] \; exp - (\lambda_1 r_1 + \lambda_2 r_2 + \lambda_3 r_3) \; dr_1 dr_2 dr_3 \qquad (6)$$

Equation (6) factorizes into the r_3 integral $\int_0^\infty r_3 2 \; e^{-2\lambda_3 r_3} dr_3 = 1/(4\lambda_3{}^3)$ and a the two-dimensional integral over r_1 and r_2. Splitting the latter into the sectors $r_1 < r_2$ and $r_1 > r_2$ and evaluating the resulting elementary radial integrals gives, for $\lambda_1 = \lambda_2 \equiv \lambda$, $\langle\phi_1|\phi_0\rangle = 35/(1024\lambda^7\lambda_3{}^3)$. This closed-form result provides a direct analytic check of the symbolic matrix-element pipeline used in Maxima. The kinetic-energy, nuclear-attraction and electron-repulsion matrix elements are generated analogously after the appropriate differential or Coulomb operator is applied.

This worked example also illustrates why the constraint $\lambda_1 = \lambda_2$ discussed in Sec. 4 is more than a matter of convenience: setting the two core parameters equal collapses what would otherwise be a two-variable rational function of λ_1 and λ_2 into

a single-variable one for every matrix element of this type, roughly halving the dimensionality of the non-linear parameter search at each stabilization step of Sec. 3.2, at the cost of the approximation quantified indirectly through the deviations reported in Sec. 5.3.

As a second consistency check, consider the uncorrelated factor ϕ_0 of Eq. (5). For a product of exponential s-type radial factors, direct integration gives the normalized kinetic-energy expectation value shown in Eq. (7). Correlation-dependent cross terms appear only when the Laplacian acts on explicit interelectronic factors such as r_{12}, and these terms are generated symbolically in the same matrix-element pipeline.

$$\langle\phi_0|\hat{T}|\phi_0\rangle \;/\; \langle\phi_0|\phi_0\rangle = 1/2(\lambda_1 2 \;+\; \lambda_2 2 \;+\; \lambda_3 2) \;-\; (\lambda_1 \;+\; \lambda_2 \;+\; \lambda_3) \tag{7}$$

Equation (7) is used only as a simple internal consistency check; all production calculations employ the complete correlated matrix elements generated from the basis of Eq. (2).

2.4. Spin Coupling and Antisymmetry

A three-electron doublet state admits two linearly independent spin-coupling schemes: the two 1s electrons may first be coupled to a singlet ($S_{12} = 0$), with the 2s electron then coupled to that singlet to give the overall doublet, or the 1s and 2s electrons may instead be coupled pairwise before the third spin is added, giving a second, linearly independent doublet spin function. Both couplings are compatible with total spin S = ½, and a fully general variational treatment would include both, with the relative weight of each determined by energy minimization; the resulting two-term spin basis is known in the literature to improve the ground-state energy over a single-spin-function treatment by an amount that is small on the absolute energy scale but not negligible at the level of precision reported in Sec. 5.3 [2, 3]. The present implementation fixes a single spin-coupling scheme — the one in which the two formally equivalent 1s electrons are coupled first — consistent with the $1s^2$ closed-shell coupling adopted in the present basis construction (Figure 1). This choice keeps the non-linear optimization of Sec. 3.2 and the symbolic matrix-element generation of Sec. 4 to a single spin sector, at the cost of leaving on the table the small additional variational freedom that a two-spin-function basis would provide; this is listed explicitly among the limitations of Sec. 5.6.

The spatial–spin part of the basis is constructed to satisfy the required permutation antisymmetry for the $(1s^2 2s)^2S$ doublet state: ϕ in Eq. (2) is built as an explicitly symmetric function of r_1 and r_2, achieved by summing the two terms with ℓ_1 and ℓ_3 interchanged, and is combined with the antisymmetric singlet spin function for that pair, so that the product of the spatial and spin parts for electrons 1 and 2 is overall antisymmetric under their exchange, as required by the Pauli principle. The construction follows the specific Hylleraas-type scheme adopted throughout Secs. 1–2 [2, 3, 6, 20, 24], in which a single doublet spin-coupling function is used rather than a full Slater-determinant antisymmetrizer over all six permutations of the three electrons; the present implementation follows this single-coupling construction rather than introducing an additional full six-permutation determinant representation, and the effect of the second, linearly independent spin-coupling scheme discussed above is left as an explicit limitation of the present work (Sec. 5.6) rather than assumed to be unimportant.

3. Complex-Rotation Formalism

3.1. Rotated Hamiltonian and Complex Eigenvalue

The complex-rotation transformation replaces each radial coordinate by $r \rightarrow r\, e^{i\theta}$, with θ a real rotation angle. Applied to the Coulombic Hamiltonian of Eq. (1), this analytic continuation gives the non-Hermitian, θ-dependent operator

$$H(\theta) \;=\; e^{-2i\theta}\;\hat{T} \;+\; e^{-i\theta}\;\hat{C} \;+\; e^{-i\theta}\;\hat{W} \tag{8}$$

where $\hat{T} = \; -1/2(\Delta_1 + \Delta_2 + \Delta_3)$ is the kinetic-energy operator, $\hat{C} = \; -Z(1/r_1 + 1/r_2 + 1/r_3)$ the electron–nucleus attraction, and $\hat{W} = \; 1/r_{12} + 1/r_{13} + 1/r_{23}$ the electron–electron repulsion. Under Aguilar–Combes–Balslev–Combes dilatation analyticity [13, 14], the spectrum of $H(\theta)$ consists of the bound-state eigenvalues of the physical ($\theta = 0$) Hamiltonian, unchanged in position, together with a continuum rotated by an angle -2θ about each ionization threshold and any resonance poles uncovered as θ is increased past the resonance's own complex phase. In the latter case the eigenvalue takes the form

$$W \;=\; \langle\Psi|H(\theta)|\Psi\rangle \;/\; \langle\Psi|\Psi\rangle \;=\; E_r \;-\; i\eta \tag{9}$$

with the real part E_r giving the resonance position and $\eta \;\equiv\; -Im\;W$ the associated imaginary component; for a genuine resonance $\eta = \Gamma_r/2$, the physical autoionization half-width, whereas for a bound state, the case of present interest, η is only a finite-basis numerical diagnostic and carries no such physical meaning (Sec. 5.5). When applied to a genuine bound state below all ionization thresholds, no resonance pole is uncovered by the rotation: the true eigenvalue remains, in exact arithmetic, a fixed real number independent of θ, and only the surrounding rotated continuum sweeps through the complex plane as θ is varied. Section 5.5 returns to the practical consequence of this distinction for the present finite-basis calculation. Throughout this paper E_r is quoted as the magnitude of the total electronic energy, $|E|$ (so that larger E_r means a more deeply bound state); this matches the convention used by every comparison study cited in Sec. 5.3 and by the source

calculation itself, and is adopted purely for ease of tabulation: the physical total energy is of course negative.

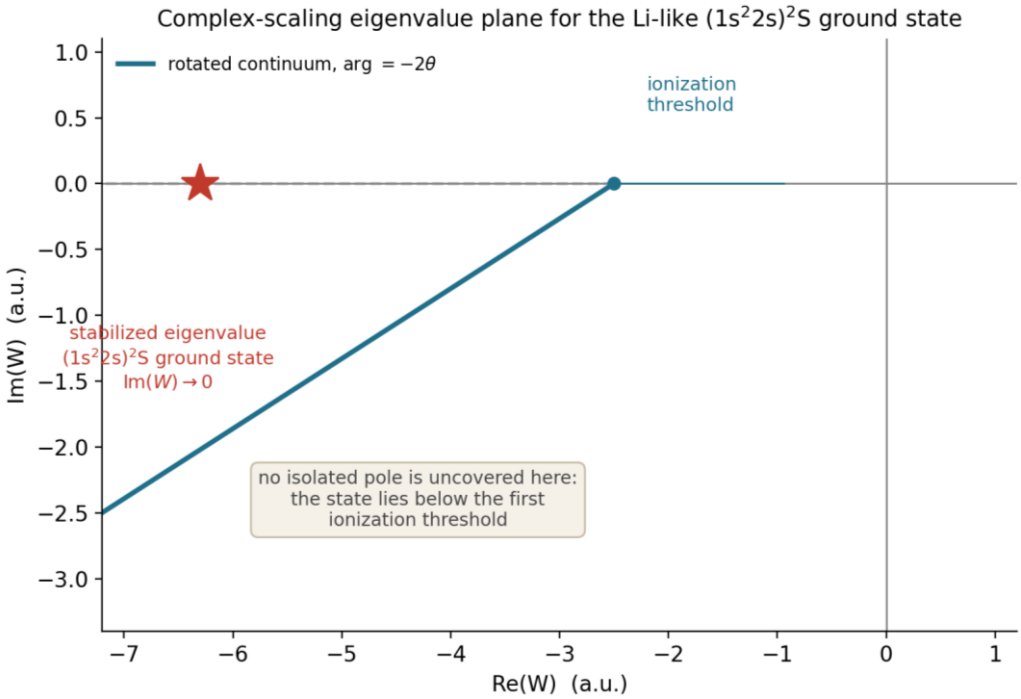

Figure 3. *Schematic complex-scaling eigenvalue plane for the $(1s^2 2s)^2S$ ground state: the rotated continuum sweeps away from the real axis by an angle -2θ about the ionization threshold, while the true ground-state eigenvalue remains on the real axis, well separated from any resonance pole.*

3.2. Stabilization Procedure

A finite correlated basis cannot reproduce the exact analytic behaviour of Sec. 3.1, and a well-converged eigenvalue must instead be identified through a three-stage stabilization procedure, following the general prescription used for autoionizing-state calculations with this method [15-21]:

(i) Real-Hamiltonian stabilization. The $\theta = 0$ Hamiltonian matrix is diagonalized as a function of the non-linear parameters λ_1, λ_2, λ_3, and the eigenvalue associated with the target $(1s^2 2s)^2S$ state is tracked until it becomes stationary with respect to small variations of these parameters — the usual variational stationarity condition, here used as a pre-selection step before rotation.

(ii) Complex rotation. The rotation angle θ is then switched on and increased from zero; the previously stabilized eigenvalue is followed as a function of θ, and a plateau in the (E_r, η) trajectory, formally, $\partial|W|/\partial\theta \approx 0$ together with $\partial|W|/\partial\lambda_i \approx 0$, is taken to signal that the finite-basis approximation to the eigenvalue has become insensitive to the auxiliary rotation angle.

(iii) Basis-size sensitivity. Steps (i)–(ii) are repeated for the available basis sizes Ω and the resulting stabilized eigenvalues are compared. For the Hermitian $\theta = 0$ problem, enlargement of a properly nested variational space is governed by the usual Ritz/Hylleraas–Undheim ordering [28]. No corresponding monotonic upper-bound statement is assumed for the complex-rotated $\theta \neq 0$ eigenvalues.

For the $\theta \neq 0$ sector, it should be stressed that the Ritz upper-bound property invoked in step (i) applies strictly only to the Hermitian, $\theta = 0$ Hamiltonian; once $\theta \neq 0$, $H(\theta)$ is non-Hermitian and the resulting complex eigenvalue is not bounded from above by a variational principle in the usual sense. Steps (ii)–(iii) are therefore treated as a stabilization/plateau search over a generalized non-Hermitian matrix eigenvalue problem rather than as conventional energy minimization. This distinction is essential when the residual imaginary components are discussed in Sec. 5.5.

4. Computational Implementation

The analytic matrix elements described in Sec. 2.3, together with the rotated Hamiltonian of Eq. (8), were implemented and evaluated in Maxima, a free computer-algebra system descended from the original MIT Macsyma project and distributed under the GNU General Public License. Maxima was chosen because the radial integrals arising from the Hylleraas basis, once reduced through the Legendre expansion of the interelectronic distances, are expressible in closed analytic form (confluent hypergeometric functions of the non-linear parameters), so that a symbolic environment avoids the discretiza-

tion error of numerical quadrature while still allowing the resulting analytic expressions to be evaluated numerically for the eigenvalue search [29].

For each nuclear charge Z, the calculation proceeds by (a) generating the full set of integer tuples (i, j, k, n, p, q) with $i + j + k + n + p + q = \Omega$, (b) constructing the corresponding normalization, kinetic-energy, nuclear-attraction and electron-repulsion matrices symbolically as functions of $\lambda_1, \lambda_2, \lambda_3$ and θ, (c) numerically diagonalizing the resulting generalized eigenvalue problem H(θ)c = WSc for trial values of the non-linear parameters, and (d) applying the three-stage stabilization procedure of Sec. 3.2 to locate the converged eigenvalue associated with the $(1s^2 2s)^2S$ state. For the three-electron systems treated here, the parameters λ_1 and λ_2 associated with the two 1s core electrons were constrained to a common value ($\lambda_1 = \lambda_2$) to reduce the dimensionality of the non-linear search, while λ_3, describing the 2s valence electron, was optimized independently; this constraint is physically motivated by the near-degeneracy of the two core electrons and mirrors the treatment adopted in earlier work on this system [17, 24].

Two basis sizes were tested for the neutral lithium atom, Ω = 9 and Ω = 12, in order to assess the sensitivity of the stabilized energy and residual imaginary component to the size of the correlated expansion (Sec. 5.1). Because Ω = 9 gave the closer agreement with the independent benchmark for Z = 3, it was adopted as the working basis for the ionic series Z = 4–8; Ω = 12 is retained only as a finite-basis sensitivity check, and only one basis size was explored for the ions; this is a genuine limitation of the present study and is discussed further in Sec. 5.6.

The number of integer tuples (i, j, k, n, p, q) satisfying with all six exponents non-negative, and hence the dimension of the Hamiltonian and overlap matrices that must be assembled and diagonalized, grows combinatorially with Ω, as the number of compositions of Ω into six non-negative parts, C(Ω+5,5). Table 1 lists this raw count for Ω = 9 through Ω = 12; it rises from 2 002 at Ω = 9 to 6 188 at Ω = 12, a factor of roughly three, even though the two basis sizes tested in Sec. 5.1 differ by only three units in Ω. In practice, the correlated basis actually retained is considerably smaller than this raw count because the parity, total angular momentum and Pauli-antisymmetry constraints built into the angular–spin factor χ of Eq. (2) eliminate a large fraction of the naively enumerated tuples before the matrix elements are ever assembled; nonetheless, the underlying growth in the number of symbolic matrix elements to be generated, simplified and evaluated is the dominant computational cost of enlarging Ω in a purely symbolic environment such as Maxima, and it is the practical reason Ω = 12 required substantially more computation, than Ω = 9. The larger symbolic problem also makes the subsequent non-Hermitian stabilization numerically more delicate, but computational cost alone is not invoked as an explanation for the Ω = 12 energy shift discussed in Sec. 5.1.

Two further practical points affect the reliability of the numerical eigenvalue search itself. First, because the matrix elements involve differences of large intermediate terms (each of the order Z^a for some exponent a, before cancellation), the symbolic-to-numeric evaluation was carried out in exact or high-precision rational arithmetic wherever Maxima's internal representation allowed it, with floating-point evaluation deferred to the final generalized-eigenvalue step, in order to limit the loss of significant digits that a purely floating-point symbolic pipeline would otherwise introduce. Second, the non-Hermitian generalized eigenvalue problem H(θ)c = WSc was solved by standard dense-matrix diagonalization at each trial (λ_1, λ_2, λ_3, θ) point along the stabilization search of Sec. 3.2, rather than by an iterative or sparse solver; this is adequate for the modest matrix dimensions reached at Ω = 9–12 but would become a limiting factor for substantially larger bases, a point returned to in Sec. 6.

Table 1. *Raw number of integer tuples (i, j, k, n, p, q) satisfying $i + j + k + n + p + q = \Omega$, before parity, angular-momentum and antisymmetry constraints are applied.*

Ω	C(Ω+5,5)
9	2 002
10	3 003
11	4 368
12	6 188

5. Results and Discussion

5.1. Convergence for Neutral Lithium

Table 2 lists the optimized parameters and stabilized eigenvalues obtained for neutral lithium with the two tested basis sizes. The Ω = 12 calculation requires a substantially larger rotation angle (θ = 0.683 rad, compared with 0.300 rad for Ω = 9) and gives a less-bound real part than Ω = 9. Against the high-precision nonrelativistic benchmark of 7.478 060 324 a.u. [9, 10, 30], Ω = 9 is the closer of the two results. This non-monotonic behaviour must not be interpreted as a failure of the underlying Hermitian variational expansion: the Ritz upper-bound property applies to the θ = 0 problem, whereas the stabilized θ ≠ 0 eigenvalue is obtained from a non-Hermitian generalized eigenvalue problem. The larger rotation angle and the increased dimension of the symbolic basis can also increase the sensitivity of the plateau search. With only two basis sizes available, however, the present data do not permit these effects to be separated quantitatively or a unique cause of the Ω = 12 shift to be established. Accordingly, Ω = 12 is retained as a sensitivity check, while Ω = 9 is used as the working basis for the isoelectronic sequence because it gives the closer neutral-lithium benchmark agreement.

The difference between the $\Omega = 9$ and $\Omega = 12$ stabilized values is therefore interpreted only as an indicator of the sensitivity of the present finite-basis stabilization procedure, not as a formal uncertainty estimate. No monotonic convergence claim is made for the complex-scaled eigenvalues, and no extrapolation is attempted from two basis sizes. This conservative interpretation is consistent with the non-Hermitian character of $H(\theta)$ at $\theta \neq 0$ and with the explicit limitations stated in Sec. 5.6.

Table 2. *Optimized non-linear parameters and stabilized ground-state energy for the lithium atom ($Z = 3$) with basis sizes $\Omega = 9$ and $\Omega = 12$. $-\mathrm{Im}\ W$ is reported rather than $\Gamma/2$ as a reminder that, for this bound state, the quantity is a numerical diagnostic rather than a physical resonance half-width (Sec. 5.5); for a genuine resonance the two coincide, $\Gamma/2 = -\mathrm{Im}\ W$.*

Ω	θ	$\lambda_1 = \lambda_2$	λ_3	E_r (a.u.)	$-\mathrm{Im}\ W$ (a.u.)
9	0.300	6.850	0.282	7.478 037 45	0.660 17
12	0.683	6.850	0.282	7.477 696 61	0.945 45

5.2. Energies Along the Isoelectronic Sequence

Table 3 collects the $\Omega = 9$ results for the five ionic members of the sequence, Be^+ through O^{5+}. The total energy grows in magnitude from 14.32 a.u. for Be^+ to 64.23 a.u. for O^{5+}, tracking the increasingly strong nuclear attraction, while the core parameters $\lambda_1 = \lambda_2$ rise almost linearly with Z (from 8.558 to 13.633), consistent with a steadily contracting $1s^2$ shell. The valence parameter λ_3, by contrast, stays confined to a narrow range around 0.27–0.35 across the whole series, with no clear monotonic trend, a point taken up in Sec. 5.4. Figure 4 plots E_r against Z for the full sequence including the neutral atom.

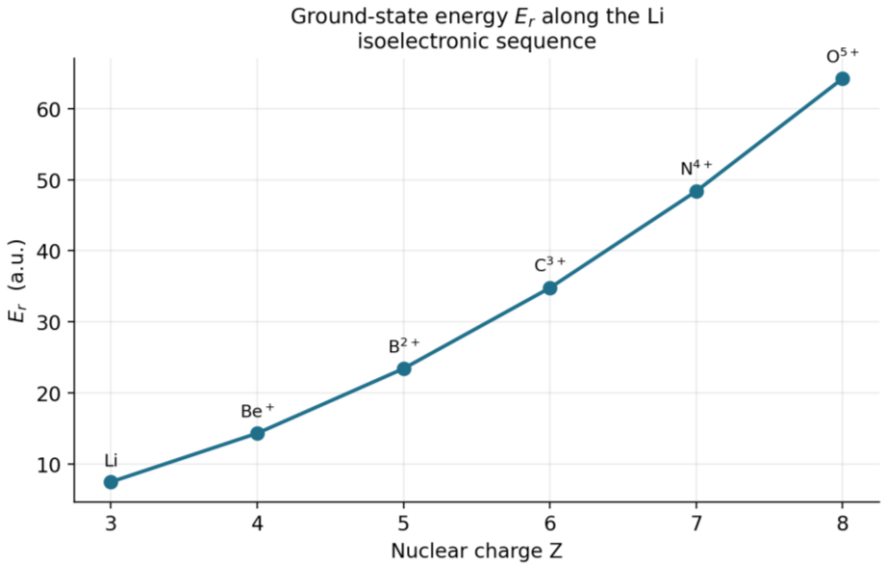

Figure 4. *Ground-state energy E_r of the $(1s^2 2s)^2S$ state as a function of the nuclear charge Z along the lithium isoelectronic sequence, $\Omega = 9$ for all points.*

Table 3. *Optimized non-linear parameters and stabilized ground-state energy for the lithium-like ions Be^+–O^{5+} ($Z = 4$–8), basis size $\Omega = 9$. As in Table 2, $-\mathrm{Im}\ W$ is a numerical diagnostic, not a resonance half-width (Sec. 5.5).*

Z	Ion	θ	$\lambda_1 = \lambda_2$	λ_3	E_r (a.u.)	$-\mathrm{Im}\ W$ (a.u.)
4	Be^+	0.40	8.558	0.266	14.324 269	0.447 02
5	B^{2+}	0.50	9.981	0.307	23.425 215	1.151 78

Z	Ion	θ	$\lambda_1 = \lambda_2$	λ_3	E_r (a.u.)	−Im W (a.u.)
6	C^{3+}	0.60	11.125	0.300	34.776 775	5.110 37
7	N^{4+}	0.70	12.380	0.329	48.379 836	11.659 38
8	O^{5+}	0.80	13.633	0.350	64.225 096	21.916 32

5.3. Comparison with Independent Literature Values

Table 4 compares the present energies with five independent sets of literature values spanning several distinct methodologies: the large multiple-basis-set Hylleraas expansions of Yan, Tambasco and Drake [4], the compact 20–50-term Hylleraas wave functions of Thakkar and coworkers [6], the full-core-plus-correlation configuration-interaction results of Chung [5], the 60–92-term Hylleraas calculations of Ho [31], and the semi-empirical screening-constant-by-unit-nuclear-charge (SCUNC) values of Sakho [32]. Across Z = 3–8, the relative deviation from the Yan et al. benchmark remains below 0.0061% (Figure 5 and Table 5). The present Ω = 9 expansion is therefore treated as a restricted compact working basis; no direct claim is made that its cardinality is smaller than that of Ref. [24], because the two studies use different basis constructions and counting conventions. The Ho values, obtained from an independently optimized 60–92-term Hylleraas basis, are systematically the most tightly bunched with the present results for the neutral atom, while the semi-empirical Sakho values show the largest and most rapidly growing deviation with Z, consistent with the intrinsically lower accuracy expected of a screening-constant parametrization relative to fully correlated variational methods.

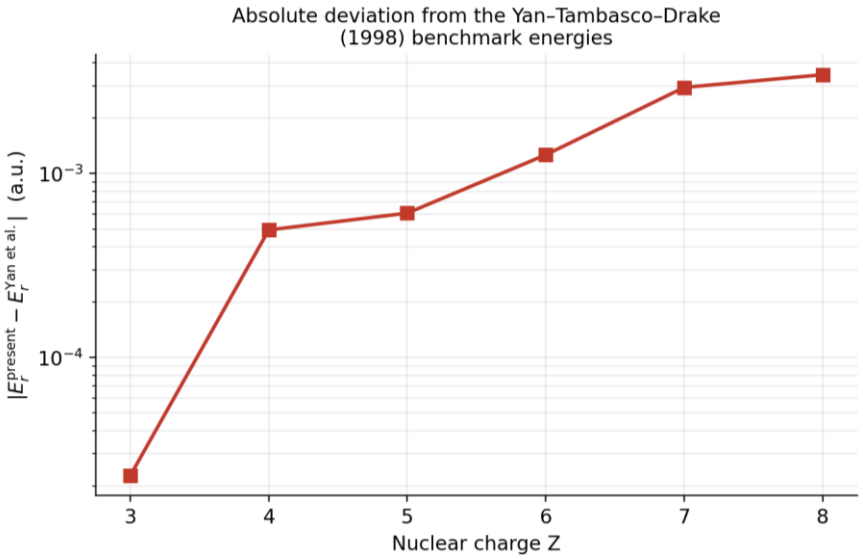

Figure 5. *Absolute deviation of the present energies from the Yan–Tambasco–Drake (1998) benchmark values, plotted on a logarithmic scale against nuclear charge Z.*

Table 4. *Comparison of the present total energies E_r (a.u.) with independent literature values for the $(1s^2 2s)^2S$ ground state of the Li isoelectronic sequence, Z = 3–8.*

Z	Present work	Sakho [32]	Yan et al. [4]	Thakkar et al. [6]	Chung [5]	Ho [31]
3	7.478 037 46	7.477 749 40	7.478 060 32	7.478 059 61	7.478 059 70	7.478 031 0
4	14.324 269 2	14.325 247 98	14.324 763 18	14.324 759 26	14.324 761 00	14.324 696 0
5	23.425 215 1	23.427 743 31	23.424 605 72	23.424 603 10	23.424 603 10	23.424 523 0
6	34.776 775 1	34.781 227 32	34.775 511 28	34.775 508 35	34.775 508 20	34.775 418 0

Z	Present work	Sakho [32]	Yan et al. [4]	Thakkar et al. [6]	Chung [5]	Ho [31]
7	48.379 836 4	48.384 755 20	48.376 898 32	48.376 895 00	48.376 894 90	48.376 798 0
8	64.225 096 3	64.238 090 34	64.228 542 08	64.228 539 18	64.228 538 50	64.228 435 0

It is worth noting explicitly that the deviation from the high-precision benchmarks grows with Z (from ~2×10^{-5} a.u. at Z = 3 to ~3×10^{-3} a.u. at Z = 8), a pattern also seen, though less strongly, in Ref. [24]. A plausible contributing factor is that the shared, single $\lambda_1 = \lambda_2$ core parameter becomes a coarser approximation to the true (and increasingly contracted) 1s orbital as Z grows, while the fixed basis size $\Omega = 9$ was not re-optimized for each ion beyond the non-linear parameter search; a systematic study of basis-size convergence at fixed Ω for each Z, rather than a single value carried over from lithium, would be needed to confirm this interpretation, and is left for future work (Sec. 6).

A complementary way to read Table 4 is in relative rather than absolute terms. Table 5 expresses the same deviation from the Yan et al. benchmark as a percentage of the total energy, $|E_r^{present} - E_{r\gamma}^{an}|/|E_{r\gamma}^{an}| \times 100$. On this relative scale the picture is more stable across the sequence than the absolute deviation of Figure 5 might suggest: the relative error stays within roughly 0.0003% (Z = 3) and 0.006% (Z = 7–8), a range of only about a factor of twenty despite the total energy itself growing by close to a factor of nine over the same interval. This indicates that the compact basis preserves a relatively stable fractional accuracy in the total ground-state energy across the sequence, and that the absolute deviations of Figure 5 grow mainly because the overall energy scale grows with Z, rather than because the fractional quality of the wave function itself degrades sharply; the comparison here concerns total energies, not a separately evaluated correlation-energy decomposition.

Table 5. *Relative deviation of the present energies from the Yan–Tambasco–Drake (1998) benchmark, expressed as a percentage of the total energy.*

Z	Ion	$\lvert E_{rpresent} - E_{rYan}\rvert$ (a.u.)	Relative deviation (%)
3	Li	2.29×10^{-5}	0.000306
4	Be^{+}	4.94×10^{-4}	0.003448
5	B^{2+}	6.09×10^{-4}	0.002602
6	C^{3+}	1.26×10^{-3}	0.003634
7	N^{4+}	2.94×10^{-3}	0.006074
8	O^{5+}	3.45×10^{-3}	0.005366

5.4. Physical Trends Along the Sequence

Figure 6 traces the evolution of the three optimized non-linear parameters and of the stabilization angle θ with Z. The near-linear growth of $\lambda_1 = \lambda_2$ reflects the physically expected contraction of the $1s^2$ core under the strengthening effective nuclear attraction: as Z increases, the two inner electrons are pulled progressively closer to the nucleus, and the optimal exponential decay rate of the corresponding radial factor increases correspondingly. The comparatively flat behaviour of λ_3 is qualitatively consistent with strong screening of the 2s valence electron by this contracting core; the standard qualitative picture for alkali-like valence electrons is that the effective potential they see stays close to that of a singly-charged ion ($Z-\delta$, $\delta \approx 2$) rather than tracking the bare nuclear charge, and the weak variation of λ_3 is consistent with that picture, though λ_3 remains a variational radial-scale parameter rather than a directly measured effective charge. The rotation angle θ required to reach the stabilization plateau grows monotonically with Z, indicating that a numerically larger rotation is needed to disentangle the target eigenvalue from the increasingly compressed rotated continuum as the ion becomes more tightly bound.

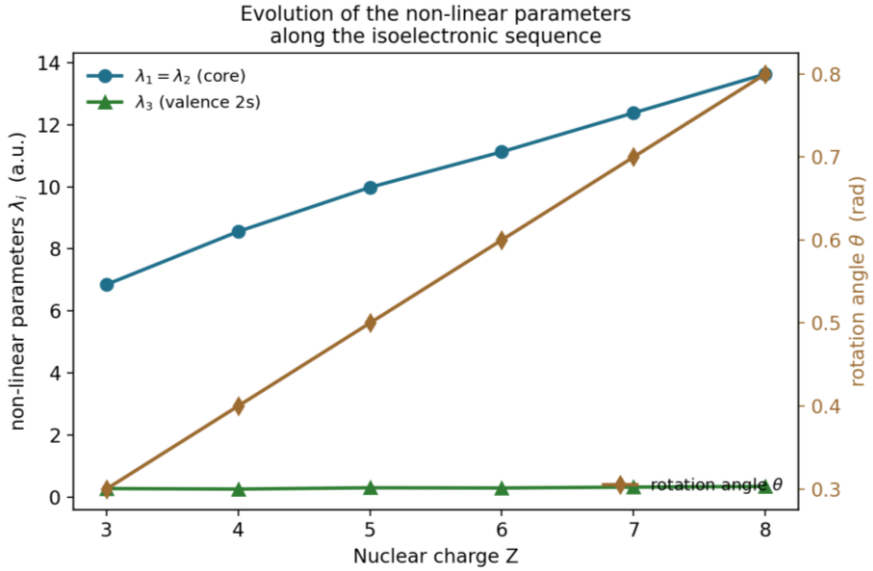

Figure 6. *Evolution of the optimized non-linear parameters $\lambda_1 = \lambda_2$ (core), λ_3 (valence), and rotation angle θ along the isoelectronic sequence, $\Omega = 9$.*

A convenient way to quantify the core-contraction trend of Figure 6 is through the ratio λ_1/Z, which measures how closely the optimized core parameter tracks the bare nuclear charge. This ratio falls from 2.28 at Z = 3 to 1.70 at Z = 8, a steady decrease rather than a constant value, showing that the core parameter grows somewhat more slowly than Z itself; this is the expected signature of the residual electron–electron repulsion within the $1s^2$ shell, which partially opposes the growing nuclear attraction and prevents λ_1 from tracking Z linearly all the way through the series. The complementary valence ratio $\lambda_3/(Z-2)$, which compares λ_3 to the charge $(Z-2)$ that a fully screened hydrogenic 2s electron would see outside a compact two-electron core, is far from constant: it falls steadily from 0.28 at Z = 3 to about 0.06 at Z = 8, decreasing markedly faster than λ_1/Z does. Because λ_3 itself stays nearly flat (Table 3) while $Z-2$ grows severalfold, this decline simply reflects the growing denominator rather than any comparable change in λ_3; read the other way, this indicates that a simple $(Z-2)$ hydrogenic screening picture becomes an increasingly poor quantitative estimate of the radial scale of the valence electron as Z grows, though, again, λ_3 is a variational parameter rather than a directly measured effective charge, and this comparison is offered as a qualitative cross-check rather than as a determination of an effective charge.

5.5. Interpretation of the Imaginary Component: A Numerical Limitation, not a Resonance Width

Tables 2 and 3 report, alongside each stabilized energy, a nonzero imaginary component $-\mathrm{Im}\,W$ (equivalently $\Gamma/2$ for a genuine resonance) produced by the complex-rotation search. Before this quantity is discussed further, its physical status must be made explicit. Complex rotation exposes a genuine autoionization width only for a state embedded in the continuum, where analytic continuation uncovers an isolated pole of the rotated Green's function away from the real axis (Sec. 3.1, Figure 3). The $(1s^22s)^2S$ term treated in this work is not such a state: it is the true ground state of each ion, lying below the first ionization threshold, and in the exact theory its eigenvalue is real and independent of θ. The nonzero η values obtained here are therefore not a physical resonance half-width but a numerical artifact of applying a finite, resonance-oriented correlated basis and a nonzero rotation angle to a state that does not, in the exact theory, possess one; they should be read as a measure of the residual sensitivity of the finite-basis stabilized eigenvalue to the auxiliary rotation angle θ, rather than as a decay rate or a spectroscopic linewidth. Consistent with this reading, η grows sharply along the sequence (from 0.45 a.u. for Be^+ to nearly 22 a.u. for O^{5+}, Table 3) in a way that has no counterpart in the essentially featureless, long-lived ground states of these ions, and is instead symptomatic of the increasingly large rotation angle θ needed at higher Z (Sec. 5.4) pushing the finite basis further from the regime in which the stabilization plateau is sharp. For this reason, the present study reports η only as a numerical diagnostic, and none of the physical conclusions drawn in Secs. 5.2–5.4 rest on treating it as a measured linewidth.

5.6. Computational Limitations

Four limitations of the present implementation should be stated plainly. First, only a single basis size ($\Omega = 9$) was explored for the ionic series Z = 4–8, so the basis-size convergence study carried out for neutral lithium (Sec. 5.1) was not repeated ion by ion; the growing deviation from the literature benchmarks noted in Sec. 5.3 may partly reflect this. Second, the constraint $\lambda_1 = \lambda_2$ imposed on the two core parameters,

while physically motivated and computationally necessary to keep the non-linear optimization tractable in a symbolic environment, is itself an approximation whose effect on the extracted energy was not separately quantified. Third, the single-spin-coupling-scheme restriction discussed in Sec. 2.4 leaves unexplored the small additional variational freedom that a genuinely two-term spin basis would provide, and may itself contribute to the residual deviation from the literature benchmarks quantified in Table 5. Fourth, and most importantly, the interpretive limitation discussed in Sec. 5.5 means that the present $\eta = -\mathrm{Im}\ W$ values carry no independent physical linewidth information; only the real part of the stabilized eigenvalue, E_r, should be regarded as the primary numerical result of this study. None of these four limitations is fundamental to the method itself; each identifies a specific, well-defined direction in which the present implementation could be extended, and Sec. 6 returns to them explicitly.

6. Conclusion and Perspectives

A correlated Hylleraas-type variational basis, combined with the complex-rotation transformation and implemented symbolically in Maxima, has been used to compute the non-relativistic ground-state energy of the $(1s^2 2s)^2S$ term for the lithium atom and five isoelectronic ions (Be^+–O^{5+}). With a modest basis size ($\Omega = 9$), the resulting energies agree with several independent high-precision literature values: Yan, Tambasco and Drake; Thakkar and coworkers; Chung; and Ho, with relative deviations below 0.0061% across Z = 3–8, and reproduce the expected physical trend of a contracting $1s^2$ core accompanied by a comparatively stable, screened 2s valence orbital. At the same time, the study has been explicit about where the method is used outside its natural domain: because the target state lies below the ionization threshold rather than in the continuum, the imaginary part produced by the rotation procedure cannot be given a resonance-width interpretation, and is reported here only as a numerical diagnostic. The work should accordingly be read as a validation, on a specific and physically transparent bound state, of a complex-rotation-based Hylleraas implementation that is more naturally suited to genuine autoionizing resonances, including the doubly-excited states this research group and its precedent study [24] have treated elsewhere, and as an assessment of its behaviour and limitations when applied to a ground state instead.

Several extensions follow naturally from the present implementation, corresponding directly to the four limitations identified in Sec. 5.6. First, a systematic basis-size convergence study repeated independently for each ion, rather than the single $\Omega = 9$ basis carried over from lithium, would clarify whether the growing deviation from the literature benchmarks at higher Z (Sec. 5.3, Table 5) is a basis-size effect, a consequence of the shared core parameter $\lambda_1 = \lambda_2$, or both; disentangling these two contributions would most naturally be done by first relaxing $\lambda_1 = \lambda_2$ at fixed Ω and separately by increasing Ω at fixed $\lambda_1 = \lambda_2$, rather than varying both simultaneously as in the present study. Second, including the second, linearly independent spin-coupling function identified in Sec. 2.4 alongside the one used here would test directly whether the residual deviations of Table 5 are sensitive to this choice, at the cost of doubling the size of the spin sector entering the non-linear optimization. Third, extending the calculation to genuinely doubly- and singly-excited $(1s^2 ns)^2S$ and $(1s^2 2snp)^2P^\circ$ states, where complex rotation is applied to states that are true resonances rather than to the ground state, would allow a direct test of the same trial-function architecture in the regime for which the method was originally developed, would give the imaginary part of Eq. (9) its intended physical meaning as an autoionization half-width rather than the numerical diagnostic discussed in Sec. 5.5, and would connect more directly with the resonance-parameter studies already carried out by this research group [17-21] and with the excited-state results of Ref. [24]. Fourth, relativistic and QED corrections, of the size documented for this sequence by Puchalski and Pachucki [33], become non-negligible for the higher-Z members treated here and would be needed for a genuinely spectroscopic-accuracy comparison with experiment rather than with other nonrelativistic calculations. Recent studies illustrate both directions: Nader and Rubenstein [11] optimized ultra-compact explicitly correlated wave functions along the Li isoelectronic sequence, while Wan et al. [12] examined modern Breit and QED corrections for Li-like ions.

Beyond these four specific points, porting the present Maxima implementation to a compiled numerical environment, retaining the symbolic derivation of the matrix elements of Sec. 2.3 as a one-time step, but evaluating them numerically at each stabilization point of Sec. 3.2 in compiled rather than interpreted arithmetic, would allow substantially larger basis sizes to be explored at each Z individually, at a computational cost that the combinatorial growth quantified in Table 1 makes prohibitive within a purely symbolic workflow beyond $\Omega \approx 12$–15. Taken together, these directions define a concrete programme for turning the present bound-state validation into the same kind of resonance-parameter study, at comparable or better precision, that this research group has previously carried out for two-electron doubly-excited states [17-21] and, for the three-electron ground and excited states considered here, in Ref. [24].

Abbreviations

a.u.	Atomic Units (Hartree Atomic Units)
FCPC	Full-Core-Plus-Correlation (Configuration-Interaction Method, Sec. 5.3)
SCUNC	Screening Constant by Unit Nuclear Charge (Semi-Empirical Method, Sec. 5.3)
QED	Quantum Electrodynamics
GNU	GNU ("GNU's Not Unix"); here, the GNU General Public License Under Which Maxima is Distributed
MIT	Massachusetts Institute of Technology (Origin of the Macsyma Computer-Algebra Project, Sec. 4)

IOP Institute of Physics (Publishing)

Author Contributions

Youssou Gning: Conceptualization, Formal Analysis, Investigation, Writing – original draft

Mame Diarra Dieng: Conceptualization, Formal Analysis, Investigation, Writing – original draft

Moussa Toure: Formal Analysis, Investigation, Writing – original draft

Demba Sylla: Formal Analysis, Validation, Writing – original draft

Mamadou Lamine Samb: Methodology, Supervision, Validation, Writing – review & editing

Conflicts of Interest

The authors declare no conflicts of interest.

Appendix

Symbols

Z	Nuclear Charge
r_1, r_2, r_3	Radial Distances of Electrons 1, 2, 3 from the Nucleus
r_{12}, r_{13}, r_{23}	Interelectronic Distances
$\lambda_1, \lambda_2, \lambda_3$	Non-Linear Screening Parameters ($\lambda_1 = \lambda_2$ for the Two 1s Core Electrons)
i, j, k, n, p, q	Integer Exponents Defining One Correlated Basis Function
μ ≡ (i,j,k,n,p,q)	Shorthand Label for One Basis Function, φ_μ, with Coefficient c_μ
Ω	Basis-Size Cutoff, i + j + k + n + p + q = Ω
θ	Complex-Rotation Angle
H(θ)	Complex-Rotated Hamiltonian
$W = E_r - i\eta$	Complex Eigenvalue of H(θ)
E_r	Real Part of W (Energy)
η ≡ −Im W	Imaginary Part of W; $\eta = \Gamma_r/2$ for a Genuine Resonance, but a Finite-Basis Numerical Diagnostic (not a Physical Width) for the Bound State Studied here

References

[1] E. A. Hylleraas, "Neue Berechnung der Energie des Heliums im Grundzustande, sowie des tiefsten Terms von Ortho-Helium," Z. Phys. 54, 347–366 (1929). https://doi.org/10.1007/57

[2] S. Larsson, "Calculations on the Ground State of the Lithium Atom Using Wave Functions of Hylleraas Type," Phys. Rev. 169, 49 (1968). https://doi.org/10.1103/PhysRev.169.49

[3] F. W. King, "Calculations on the ground states of some members of the Li I isoelectronic series," Phys. Rev. A 40, 1735 (1989). https://doi.org/10.1103/PhysRevA.40.1735

[4] Z.-C. Yan, M. Tambasco, and G. W. F. Drake, "Energies and oscillator strengths for lithiumlike ions," Phys. Rev. A 57, 1652 (1998). https://doi.org/10.1103/PhysRevA.57.1652

[5] K. T. Chung, "Ionization potential of the lithium-like $1s^2 2s$ states from lithium to neon," Phys. Rev. A 44, 5421 (1991). https://doi.org/10.1103/PhysRevA.44.5421

[6] A. J. Thakkar, T. Koga, T. Tanabe, and H. Teruya, "Compact Hylleraas-type wave functions for the lithium isoelectronic sequence," Chem. Phys. Lett. 366, 95–99 (2002). https://doi.org/10.1016/S0009-2614(02)01544-0

[7] K. T. Chung and X.-W. Zhu, "Inequalities of the electron density at the nucleus and radial expectation values of the ground state for the lithium isoelectronic sequence," Phys. Scr. 48, 292–296 (1993).

[8] M. Godefroid, C. Froese Fischer, and P. Jönsson, "Non-relativistic variational calculations of atomic properties in Li-like ions: Li I to O VI," J. Phys. B 34, 1079 (2001). https://doi.org/10.1088/0953-4075/34/6/308

[9] D. K. McKenzie and G. W. F. Drake, "Variational calculation for the ground state of lithium and the QED corrections for Li-like ions," Phys. Rev. A 44, R6973 (1991). https://doi.org/10.1103/PhysRevA.44.R6973

[10] Z.-C. Yan and G. W. F. Drake, "Eigenvalues and expectation values for the 1^2S, 1^2P, and 1^2D states of lithium," Phys. Rev. A 52, 3711 (1995). https://doi.org/10.1103/PhysRevA.52.3711

[11] D. J. Nader and B. M. Rubenstein, "VMC optimization of ultra-compact, explicitly-correlated wave functions of the Li isoelectronic sequence in its lowest 1s2s2p quartet state," Chem. Phys. Lett. 838, 141091 (2024). https://doi.org/10.1016/j.cplett.2024.141091

[12] J.-J. Wan, Q. Ma, Z.-Y. Wu, J. Li, B. Bai, and F. Wu, "Effects of the Breit and QED corrections on the fine structure $1s^2 2s$ $^2S_{1/2}$ and $1s^2 2p$ $^2P_{1/2,3/2}$ in the lithium isoelectronic sequence," At. Data Nucl. Data Tables 166, 101757 (2025). https://doi.org/10.1016/j.adt.2025.101757

[13] J. Aguilar and J. M. Combes, "A class of analytic perturbations for one-body Schrödinger Hamiltonians," Commun. Math. Phys. 22, 269–279 (1971). https://doi.org/10.1007/BF01877510

[14] E. Balslev and J. M. Combes, "Spectral properties of many-body Schrödinger operators with dilatation-analytic interactions," Commun. Math. Phys. 22, 280–294 (1971). https://doi.org/10.1007/BF01877511

[15] Y. K. Ho, "The method of complex coordinate rotation and its applications to atomic collision processes," Phys. Rep. 99, 1–68 (1983). https://doi.org/10.1016/0370-1573(83)90112-6

[16] W. P. Reinhardt, "Complex coordinates in the theory of atomic and molecular structure and dynamics," Annu. Rev. Phys. Chem. 33, 223–255 (1982). https://doi.org/10.1146/annurev.pc.33.100182.001255

[17] A. Wague, "Application of the diagonalization approximation to the n = 3 resonant photoionization of helium-like systems," Z. Phys. D 6, 337 (1987).

[18] N. A. B. Faye and A. Wague, "Doubly-excited state resonances of the helium-like nitrogen ion N^{5+} near the n = 3 threshold of N^{6+}," Z. Phys. D 31, 37 (1994).

[19] M. Biaye, A. Konte, N. A. B. Faye, and A. Wague, "Resonance parameters of doubly excited states in two-electron systems," Eur. Phys. J. D 13, 21 (2001).

[20] M. Biaye, M. Dieng, I. Sakho, and A. Wague, "Resonance parameters of doubly-excited states in three-electron systems," Chin. J. Phys. 47, 166 (2009).

[21] Y. Gning, M. Sow, A. Traore, M. Dieng, B. Diakhate, M. Biaye, and A. Wague, "Resonance parameters of doubly excited states in helium-like ions," Radiat. Phys. Chem. 106, 1 (2015).

[22] V. V. Balashov, S. L. Grishanova, I. M. Kruglova, and V. S. Senashenko, "Resonance photoionisation of helium and helium-like ions," Opt. Spectrosc. 28, 859 (1970).

[23] U. Fano, "Correlations of two excited electrons," Rep. Prog. Phys. 46, 97 (1983). https://doi.org/10.1088/0034-4885/46/2/001

[24] B. Diop, Y. Gning, M. Faye, A. Diouf, B. Sow, M. Sow, M. Dieng, and M. Biaye, "The Ground State $(1s^22s)^2S$ and the Low-lying Excited $(1s^2ns)^2S$ States Energy Calculations of Li-Like Ions Using Special Forms of the Hylleraas-Type Wave Functions," Int. J. High Energy Phys. 7(1), 1–7 (2020). https://doi.org/10.11648/j.ijhep.20200701.11

[25] Z.-W. Wang, X.-W. Zhu, and K. T. Chung, "Energy of $1s^2ns$ (n = 3, 4 and 5) states for the lithium isoelectronic sequence," Phys. Rev. A 46, 6914 (1992). https://doi.org/10.1103/PhysRevA.46.6914

[26] H. A. Bethe and E. E. Salpeter, Quantum Mechanics of One- and Two-Electron Atoms (Springer, Berlin, 1957).

[27] A. J. Thakkar, Quantum Chemistry: A Concise Introduction for Students of Physics, Chemistry, Biochemistry and Materials Science, 3rd ed. (IOP Publishing, Bristol, 2021).

[28] E. A. Hylleraas and B. Undheim, "Numerische Berechnung der 2S-Terme von Ortho- und Par-Helium," Z. Phys. 65, 759 (1930). https://doi.org/10.1007/BF01397263

[29] Maxima, a Computer Algebra System, version 5.21.1, http://maxima.sourceforge.net/ (free software under the GNU General Public License).

[30] J. S. Sims and S. A. Hagstrom, "Hylleraas-configuration-interaction study of the 2^2S ground state of neutral lithium," Phys. Rev. A 80, 052507 (2009). https://doi.org/10.1103/PhysRevA.80.052507

[31] Y. K. Ho, "Improved Hylleraas calculations for ground state energies of lithium iso-electronic sequence," Int. J. Quantum Chem. 20, 1077–1082 (1981).

[32] I. Sakho, Screening Constant by Unit Nuclear Charge Method: Calculating the Energies of Three-Electron Atomic Systems (Lithium-like Systems), Ch. 5 (Wiley, 2018); I. Sakho, Chin. J. Phys. 52, 5 (2014).

[33] M. Puchalski and K. Pachucki, "Relativistic, QED, and finite nuclear mass corrections for low-lying states of Li and Be^+," Phys. Rev. A 78, 052511 (2008). https://doi.org/10.1103/PhysRevA.78.052511